Review Article

International Journal of Natural Sciences and Interdisciplinary Research

Controlling Soft Matter Instabilities Using Artificial Intelligence

Lakshmi N. Sridhar*

Chemical Engineering Department, University of Puerto Rico, Mayaguez, USA

***Corresponding Author**
Lakshmi. N. Sridhar, Chemical Engineering Department, University of Puerto Rico, Mayaguez, USA.

Submitted: 2026, Apr 06; **Accepted:** 2026, May 01; **Published:** 2026, May 20

Citation: Sridhar, L. N. (2026). Controlling Soft Matter Instabilities Using Artificial Intelligence. *Int Nat Sci Int Rese, 1*(2), 01-15.

Abstract

This work develops a unified framework for modeling, analyzing, and controlling oscillatory instabilities in soft matter systems governed by the Navier–Stokes equations coupled with viscoelastic constitutive laws. A reduced-order model is derived using Galerkin projection, capturing the essential interaction between velocity modes and stress dynamics. Near critical conditions, the system exhibits a Hopf bifurcation, leading to a transition from steady behavior to sustained oscillations. This bifurcation is characterized using continuation analysis, confirming the presence of a limit cycle and highlighting the role of flow–stress coupling in driving instability. To regulate these dynamics, an optimal control formulation is introduced in which the bifurcation parameter is treated as a time-dependent control variable. A key contribution of this work is the incorporation of a smooth, data-driven surrogate model to approximate system stability, enabling stability-aware optimization without explicit eigenvalue computation. The resulting control strategy effectively steers the system away from unstable regimes while maintaining performance, demonstrating a balance between stability enforcement and control effort. The proposed approach integrates reduced-order modeling, bifurcation theory, and machine learning into a computationally tractable framework. This methodology provides a promising tool for managing complex nonlinear behavior in soft matter flows and has potential applications in chemical engineering, materials processing, and fluid dynamics.

Keywords: Soft Matter, Artificial Intelligence, Hopf Bifurcation, Optimal Control, Viscoelastic Flow

1. Introduction

Soft matter systems, including polymer solutions, colloidal suspensions, and other complex fluids, exhibit rich and often counterintuitive dynamical behavior due to the interplay between viscous, elastic, and inertial effects. Unlike Newtonian fluids, whose stress depends instantaneously on the rate of deformation, soft matter fluids possess internal microstructure that evolves with the flow, leading to memory effects, nonlinear stress responses, and flow-induced instabilities. These characteristics are commonly modeled by augmenting the classical Navier–Stokes equations with additional constitutive relations, such as the Oldroyd-B model, which introduces a dynamically evolving stress tensor to capture viscoelastic behavior. As a result, the governing equations form a coupled nonlinear system in which velocity and stress interact in a highly nontrivial manner.

One of the most important consequences of this coupling is the emergence of dynamic instabilities, including oscillations and bifurcations. In particular, Hopf bifurcations play a central role in soft matter flows, marking the transition from steady-state behavior to time-periodic oscillations. These oscillations can manifest as fluctuations in velocity, stress, or other physical quantities and are often associated with undesirable phenomena such as flow-induced vibrations, reduced transport efficiency, or unstable processing conditions in chemical and biological systems. Understanding the mechanisms that lead to such instabilities, as well as developing strategies to control or suppress them, is therefore of significant practical and theoretical interest.

Due to the complexity of the full governing equations, reduced-order modeling techniques are often employed to capture the essential

dynamics of the system. One widely used approach is Galerkin projection, in which the governing partial differential equations are projected onto a small set of basis functions, yielding a low-dimensional system of ordinary differential equations. These reduced models retain the key nonlinear interactions responsible for instability while being computationally tractable for analysis and control. Near critical points, such as Hopf bifurcations, further simplification is possible using center manifold theory, which reduces the system to its most dynamically relevant modes. This leads to a normal-form representation that captures the onset of oscillations and provides a convenient framework for bifurcation analysis. Bifurcation analysis tools, such as MATCONT, enable systematic identification of qualitative changes in system behavior as parameters vary. In particular, these tools allow the detection of Hopf bifurcation points, where a pair of complex conjugate eigenvalues crosses the imaginary axis, leading to the formation of limit cycles. While such analysis is invaluable for understanding system dynamics, incorporating stability considerations directly into control design remains a challenging problem. Traditional optimal control formulations focus on minimizing performance objectives but do not explicitly account for stability boundaries, which can result in trajectories that approach or cross into unstable regions.

To address this challenge, this work integrates bifurcation analysis with optimal control in a unified framework. The reduced-order model derived from the Navier–Stokes equations and constitutive relations is first analyzed to identify Hopf bifurcation behavior. A stability dataset is then generated using continuation methods, and a neural network surrogate is trained to approximate the maximum real part of the system eigenvalues as a smooth function of the state and control variables. This surrogate is embedded within a dynamic optimization framework using Pyomo.DAE, allowing stability to be enforced through a differentiable penalty term without explicitly computing eigenvalues during optimization.

The resulting methodology provides a computationally efficient approach to stability-aware optimal control of soft matter systems. By combining physics-based modeling, bifurcation theory, and machine learning, the framework enables the design of control strategies that not only optimize performance but also avoid undesirable oscillatory behavior. This approach is particularly relevant for applications in chemical engineering, materials processing, and fluid mechanics, where maintaining stable operation is critical. The contributions of this work include the systematic derivation of a reduced-order model that captures viscoelastic instabilities, the integration of neural network-based stability prediction, and the development of an optimal control formulation that steers the system away from Hopf bifurcations.

2. Literature Review

Recent advances in soft matter and complex fluid dynamics have highlighted the importance of nonlinear interactions between flow, microstructure, and stress, particularly in systems exhibiting viscoelastic behavior. Early modern contributions emphasized the role of confinement and microstructural rearrangements in determining nonlinear flow responses in colloidal systems [1]. In parallel, other researhcers investigated instabilities in viscoelastic channel flows, demonstrating how elastic stresses can destabilize otherwise laminar configurations [2]. Complementing these studies, Carlos R. Lopez-Barron and Norman J. Wagner provided detailed insight into structure–property relationships in complex fluids, linking microscopic interactions to macroscopic rheological behavior [3].

The understanding of instabilities in soft matter systems was further advanced by Suzanne J. Haward and Gareth H. McKinley , who reviewed elastic instabilities in viscoelastic flows [4]. Suzanne M. Fielding examined shear banding phenomena in soft glassy materials [5]. At the same time, Victor Steinberg provided a comprehensive overview of elastic turbulence, a hallmark of strongly nonlinear viscoelastic flows [6]. Experimental and numerical studies by Yun Zhang and Paulo E. Arratia further demonstrated the emergence of flow instabilities in complex fluids, while Thibaut Divoux, Marc-Antoine Fardin, and Sébastien Manneville explored rheological chaos in soft materials [7,8]. Similarly, Guillaume Ovarlez and Sylvain Cohen-Addad investigated yield stress fluids, highlighting their complex flow instabilities [9].

More recent work has focused on detailed characterization of nonlinear and elastic instabilities. For example, Bo Qin and Paulo E. Arratia studied elastic instabilities in viscoelastic flows, while Dimitrios Fraggedakis et al. examined nonlinear dynamics in viscoelastic systems [10,11]. Sujoy S. Datta further elucidated the microscopic origins of soft matter flow behavior, and D.M. Walkama et al. analyzed instabilities in confined geometries [12,13]. Additionally, Y. Li and H. Zhang investigated bifurcation behavior in complex fluids, while C. Perge et al. studied colloidal suspension dynamics under flow conditions [14,15].

Benoît Saint-Michel et al. extended their earlier work to Couette flow configurations, further characterizing elastic instabilities, while V.A.H. Boudara et al. explored nonlinear viscoelastic flow instabilities [16,17]. Sujoy S. Datta et al. reported on flow-induced structures in soft materials, highlighting the coupling between microstructure and macroscopic dynamics [18]. At the same time, Y. Song et al. introduced machine learning approaches for soft matter rheology, while Y. Liu et al. developed neural network models for viscoelastic flows, demonstrating the growing importance of data-driven techniques [19.20].

Recent developments in 2024 and beyond continue to expand this field. R. Gupta et al. proposed data-driven frameworks for modeling soft matter dynamics, while Alexander Morozov and Wim van Saarloos provided a comprehensive analysis of subcritical instabilities in viscoelastic flows[21,22]. Paulo E. Arratia et al. reviewed recent advances in elastic turbulence, and X. Zhang et al. examined stability in viscoelastic channel flows [23,24]. Finally, A. Singh et al. explored optimal control strategies for instabilities in soft matter systems, highlighting the increasing integration of control theory with soft matter physics [25].

Overall, the literature demonstrates a clear progression from experimental and theoretical studies of viscoelastic instabilities toward data-driven modeling and control-oriented approaches. The present work builds on these developments by integrating reduced-order modeling, Hopf bifurcation analysis, and machine-learning-assisted optimal control into a unified framework for stability-aware control of soft matter systems.

3. Main Objective of this Work

The main objective of this work is to develop a unified, computationally efficient framework for modeling, analyzing, and controlling oscillatory instabilities in soft-matter fluid systems. Specifically, the study aims to capture the essential dynamics of viscoelastic flows by deriving a reduced-order model from the Navier–Stokes equations coupled with an appropriate constitutive law, and to use this model to investigate the onset of Hopf bifurcations. A key goal is to bridge the gap between bifurcation analysis and optimal control by incorporating stability considerations directly into the control formulation.

To achieve this, the work seeks to identify critical parameter regimes where the system transitions from stable behavior to oscillatory dynamics and to design control strategies that can prevent or regulate such transitions. An important component of the methodology is the use of a data-driven surrogate model to approximate stability metrics, thereby avoiding the computational burden of repeated eigenvalue calculations within the optimization loop. This enables the formulation of a smooth and tractable optimal control problem that can be solved efficiently. Overall, the objective is to demonstrate that stability-aware control of soft matter systems is both feasible and practical, and that combining reduced-order modeling, bifurcation theory, and machine learning provides a powerful approach for managing complex nonlinear dynamics in engineering applications. The paper is organized as follows. The literature review and model equations are first described, followed by the numerical procedures, results, discussion, and conclusions.

4. Model Equations

Soft matter fluids, such as polymer solutions and colloidal suspensions, cannot be accurately described using the classical Newtonian constitutive relation. Instead, their behavior arises from additional stress contributions that evolve dynamically with the flow. A common starting point for modeling such systems is the incompressible Navier–Stokes equations augmented with a constitutive law for the extra stress. For an incompressible fluid, the continuity and momentum balance equations are

$$\begin{aligned} &\nabla .u = 0 \\ &\rho(\frac{\partial u}{\partial t} + u.\nabla u) = -\nabla p + \nabla .\tau \end{aligned} \tag{1}$$

where ρ is the fluid density, p is the pressure, and $\boldsymbol{\tau}$ is the total extra stress tensor. In soft matter systems, the stress is decomposed into a solvent contribution and a polymer contribution as

$$\tau = \tau_s + \tau_p \tag{2}$$

The solvent part is assumed to be Newtonian and is expressed as

$$\tau_s = \mu_s(\nabla u + (\nabla u)^T) \tag{3}$$

where μ_s is the solvent viscosity.
The polymer contribution accounts for elastic effects and is governed by a constitutive equation. In the Oldroyd–B model, the polymer stress satisfies

$$\tau_p + \lambda \overset{\nabla}{\tau}_p = \mu_p(\nabla u + (\nabla u)^T) \tag{4}$$

where λ is the relaxation time of the polymer and μ_p is the polymer viscosity contribution. $\overset{\nabla}{\tau}_p$ is the upper-convected derivative of the polymer stress tensor τ_p and describes how the polymer-induced stress in a soft matter fluid evolves while being carried, stretched, and rotated by the flow.
Mathematically, it is defined as:

$$\overset{\nabla}{\tau}_p = \frac{\partial \tau_p}{\partial t} + u.\nabla \tau_p - (\nabla u)^T \tau_p - \tau_p (\nabla u) \tag{5}$$

In this equation $\frac{\partial \boldsymbol{\tau}_p}{\partial t}$ represents the local time change of polymer stress, $\mathbf{u} \cdot \nabla \boldsymbol{\tau}_p$ is the transport of stress by the moving fluid while -$(\nabla \mathbf{u})^T \boldsymbol{\tau}_p$ and -$\boldsymbol{\tau}_p (\nabla \mathbf{u})$ represent the corrections for rotation and stretching of fluid elements. $\overset{\nabla}{\tau}_p$ represents the rate of change of the polymer stress following a deforming fluid element, ensuring the model correctly captures elasticity and memory effects in soft-matter systems such as polymer solutions and viscoelastic fluids. It indicates how polymer stress evolves as it is advected, stretched, and rotated by the flow. This expression extends the ordinary time derivative by accounting for both the transport and deformation of stress within the fluid. The first term represents the local rate of change of stress at a fixed point in space, while the second term accounts for advection of stress by the velocity field **u**. The last two terms correct for distortions caused by the velocity gradients, ensuring that the stress transformation remains objective under rotations and deformations of the fluid element. Physically, this operator describes how stresses embedded in a material element evolve as it is carried, stretched, and rotated by the flow, which is essential for accurately modeling viscoelastic and soft-matter systems where memory and elasticity play significant roles.

The full governing system, therefore, consists of the incompressibility condition, the momentum equation with total stress contribution, and the constitutive equation for the polymer stress. This coupled system extends classical fluid mechanics by introducing an additional evolution equation for the stress that incorporates elastic effects via a relaxation time. When elasticity becomes sufficiently strong, the system can exhibit dynamic instabilities, such as oscillations and Hopf bifurcations, driven by the interaction among inertia, viscosity, and elastic stress evolution.

The whole continuity and momentum balance equation set can be rewritten as

$$\begin{aligned} &\nabla.u = 0 \\ &\rho\left(\frac{\partial u}{\partial t} + u.\nabla u\right) = \mu_s(\nabla^2 u) - \nabla p + \nabla.\tau_p \\ &\tau_p + \lambda \overset{\nabla}{\tau}_p = \mu_p(\nabla u + (\nabla u)^T) \end{aligned} \tag{6}$$

The reduced PDE system would be

$$\begin{aligned} &\rho\left(\frac{\partial u}{\partial t} + \frac{u\partial u}{\partial x}\right) = \mu_s \frac{(\partial^2 u)}{\partial z^2} + \left(\frac{\partial \tau_p}{\partial z}\right) \\ &\tau_p + \lambda\left(\frac{\partial \tau_p}{\partial t} + u\frac{\partial \tau_p}{\partial x} - \tau_p \frac{\partial u}{\partial x}\right) = \mu_p \frac{\partial u}{\partial z} \end{aligned} \tag{7}$$

Choosing

$$\begin{aligned} &u(x,z,t) = a_1(t)\sin\left(\frac{\pi z}{H}\right) + a_2(t)\sin\left(\frac{2\pi z}{H}\right) \\ &\tau_p(x,z,t) = a_3(t)\sin\left(\frac{\pi z}{H}\right) \end{aligned} \tag{8}$$

a_1, a_2 are the velocity amplitudes [m/s] while a_3 is the stress amplitude [Pa] . H is the characteristic length of the flow domain in the wall-normal direction.
For the momentum equation, multiplying by sin($\pi z/H$), and integrating yields

$$\frac{da_1}{dt} = -\upsilon(\frac{\pi}{H})^2 a_1 - \gamma a_2 a_1 + \kappa a_3$$
$$\frac{da_2}{dt} = -\upsilon(\frac{2\pi}{H})^2 a_2 + \gamma a_1^2 \quad (9)$$

$\nu = \mu_s / \rho[\mathrm{m}^2/\mathrm{s}]$ is the kinematic viscosity ; $\gamma[1/\mathrm{m}]$ the nonlinear interaction coefficient and $\kappa[1/(\rho\bullet\mathrm{m})]$ = stress coupling.

Using the Galerkin basis functions $\phi_1(z) = \sin(\frac{\pi z}{H}); \phi_2(z) = \sin(\frac{2\pi z}{H}); \psi(z) = \sin(\frac{2\pi z}{H})$ we obtain the coefficients

$$\gamma = \frac{\int_0^H \sin^2(\frac{\pi z}{H})\sin(\frac{2\pi z}{H})dz}{\int_0^H \sin^2(\frac{\pi z}{H})dz}; \kappa = \frac{1}{\rho}(\frac{\int_0^H \sin(\frac{\pi z}{H})\frac{d}{dz}(\sin(\frac{2\pi z}{H})dz)}{\int_0^H \sin^2(\frac{\pi z}{H})dz}); \upsilon = \frac{\mu}{\rho} \ .$$

Doing the same for the stress equation yields

$$\frac{da_3}{dt} = -\frac{1}{\lambda}(a_3) + \eta(a_1) - \xi a_1 a_3 \quad (10)$$

Where

$$\xi = \frac{\int_0^H \sin(\frac{\pi z}{H})\sin^2(\frac{2\pi z}{H})dz}{\int_0^H \sin^2(\frac{2\pi z}{H})dz}; \eta = \mu_p(\frac{\pi}{H}) \quad (11)$$

The three obtained ODE can be succinctly written as

$$\frac{da_1}{dt} = -c_1 a_1 - c_2 a_1 a_2 + c_3 a_3$$
$$\frac{da_2}{dt} = -c_4 a_2 + c_5 a_1^2 \quad (12)$$
$$\frac{da_3}{dt} = -\frac{1}{\lambda} a_3 + c_6 a_1 - c_7 a_1 a_3$$

The parameter definitions are $c_1 = \nu(\pi/H)^2\ [1/\mathrm{s}]$; $c_4 = \nu(2\pi/H)^2\ [1/\mathrm{s}]$; c_2, c_5, $c_7[1/\mathrm{m}]$ nonlinear interaction ; $c_3[1/(\rho\bullet\mathrm{m})]$ stress → velocity coupling ; c_6[Pa/m] velocity → stress coupling ; λ[s] relaxation time . $a_1\ (t)$ and $a_2\ (t)$ represent the amplitudes of the first two velocity modes (flow structure), while $a_3\ (t)$ represents the amplitude of the polymer stress mode (the fluid's elastic response). These equations will now be made dimensionless.

To simplify the system and reveal the underlying parameter dependencies, we introduce characteristic scales. Let Udenote a characteristic velocity scale (m/s) and Ha characteristic length scale (m). A natural time scale is then given by $T = H/U$, which represents the time required for fluid to traverse the characteristic length. We now define dimensionless variables by scaling each quantity with its corresponding reference value $A_1 = \frac{a_1}{U}, A_2 = \frac{a_2}{U}, A_3 = \frac{a_3}{\rho U^2}, t^* = \frac{t}{T} = \frac{tU}{H}$.

Here, ρU^2 is used as the stress scale, consistent with inertial stress. Using the chain rule, time derivatives transform according to

$$\frac{d}{dt} = \frac{U}{H}\frac{d}{dt^*} \tag{13}$$

Applying this transformation, we substitute $a_1 = UA_1$, $a_2 = UA_2$, and $a_3 = \rho U^2 A^3$ into the first equation. The left-hand side of the first dimensional equation becomes

$$(\frac{da_1}{dt}) = \frac{U^2}{H}(\frac{dA_1}{dt^*}) \tag{14}$$

While the right-hand side becomes

$$-c_1 UA_1 - c_2 U^2 A_1 A_2 + c_3 \rho U^2 A_3. \tag{15}$$

Dividing both sides by U^2/H yields

$$(\frac{dA_1}{dt^*}) = -(\frac{c_1 H}{U})A_1 - (c_2 H)A_1 A_2 + (c_3 \rho H)A_3. \tag{16}$$

Introducing dimensionless parameters $\sigma = -\frac{c_1 H}{U}, \alpha = c_2 H, \beta = c_3 \rho H$ results in

$$(\frac{dA_1}{dt^*}) = \sigma A_1 - \alpha A_1 A_2 + \beta A_3. \tag{17}$$

Applying the same procedure to the second equation, we obtain

$$(\frac{dA_2}{dt^*}) = -(\frac{c_4 H}{U})A_2 + (c_5 H)A_1^2 \tag{18}$$

Defining $\omega = -\frac{c_4 H}{U}, \gamma = c_5 H$, we write

$$(\frac{dA_2}{dt^*}) = \omega A_2 + \gamma A_1^2 \tag{19}$$

For the third equation, substitution and simplification yield

$$(\frac{dA_3}{dt^*}) = -(\frac{H}{\lambda U})A_3 + (\frac{c_6 H}{\rho U})A_1 - (c_7 H)A_1 A_3. \tag{20}$$

Introducing $\delta = \frac{H}{\lambda U}, \eta = \frac{c_6 H}{\rho U}, \xi = c_7 H,$

we obtain

$$(\frac{dA_3}{dt^*}) = -(\delta)A_3 + (\eta)A_1 - (\xi)A_1 A_3. \tag{21}$$

The three non-dimensional ODE set (after dropping the asterik) is

$$\begin{aligned}(\frac{dA_1}{dt}) &= \sigma A_1 - \alpha A_1 A_2 + \beta A_3 \\ (\frac{dA_2}{dt}) &= \omega A_2 + \gamma A_1^2 \\ (\frac{dA_3}{dt}) &= -(\delta) A_3 + (\eta) A_1 - (\xi) A_1 A_3\end{aligned} \tag{22}$$

This transformation removes physical units from the system and expresses the dynamics in terms of dimensionless parameters, which represent ratios of physical effects such as inertia, viscosity, and elasticity. Importantly, the structure of the equations is preserved, while the key control parameters governing stability and bifurcation behavior become explicit. The parameter σ governs the linear growth of the velocity modes and serves as the primary bifurcation parameter. Physically, σ is related to the imposed flow conditions (e.g., Reynolds number or shear rate), and can therefore be interpreted as a controllable and bifurcation parameter. Typical values for the other parameters are $\beta = 1.2$, ω=-1.0, $\gamma = 1.0$, $\delta = 0.5$, $\eta = 1.0$, $\xi = 0.8$. Considering the equilibrium $A_1 = A_2 = A_3 = 0$. Linearizing the system gives

$$\frac{dA}{dt} = L(\sigma)A \tag{23}$$

Assume that at a critical value $\sigma = \sigma_c$, the linear operator has one complex conjugate pair of eigenvalues and one stable eigenvalue ($\lambda_{1,2} = \pm i\omega, \lambda_3 < 0$)

The dynamics split into a two-dimensional oscillatory part (critical modes) and a one-dimensional decaying part (stable mode). By center manifold theory, the stable variable is not independent but is determined by the critical variables. This implies that

$$A_3 = h(A_1, A_2) \tag{24}$$

and near the equilibrium this function starts at quadratic order, and hence $A_3 \approx c(A_1^2 + A_2^2)$. This means the stress mode is driven by the oscillatory modes' energy.

We define the two critical amplitudes as $A_1 = X, A_2 = Y, A_3 = Z$. The key point from the eigenvalue structure is that the linear part of the critical subsystem must form a rotation. This always has the form

$$\begin{aligned}\frac{dX}{dt} &= \sigma X - \omega Y \\ \frac{dY}{dt} &= \omega X + \sigma Y\end{aligned} \tag{25}$$

This structure appears because the eigenvalues are $\sigma \pm i\omega$, which implies coupling between X and Y. Now we substitute the center manifold approximation for the stable variable:

$$Z \approx \beta(X^2 + Y^2)$$

This is the only quadratic expression that is symmetric in X and Y, so it is the correct invariant form. Next, we include feedback from the stress variable into both critical modes. Since the original system couples A_3 into the velocity equation, this produces damping proportional to Z. Because the center manifold is symmetric, this damping must act equally on both X and Y. Combining linear rotation, growth rate, and nonlinear feedback gives

$$\frac{dX}{dt} = \sigma X - \omega Y - \alpha XZ$$
$$\frac{dY}{dt} = \omega X + \sigma Y - \alpha YZ \quad (26)$$
$$\frac{dZ}{dt} = -\delta Z + \beta(X^2 + Y^2)$$

This final system is the reduced center-manifold form of the original Galerkin model near the critical point. It contains:

- A rotational linear subsystem (X,Y) due to complex eigenvalues.
- an enslaved stable mode Zdriven by the energy $X^2 + Y^2$,
- a nonlinear damping through stress feedback.

The variable $X(t)$ represents amplitude of first velocity mode (m/s) ; $Y(t)$ is the amplitude of the second (phase-shifted) velocity mode m/s ; $Z(t)$ represents the amplitude of stress mode (Pa). t is the time in seconds. The parameter σ is the linear growth/decay rate (bifurcation parameter) 1/s ω represents the oscillation frequency (rotation rate between modes)1/s ; α is the stress–velocity coupling coefficient 1/(Pa•s) β is the energy-to-stress conversion coefficient(Pa/(m²/s²) = kg/m³). δ represents the stress relaxation rate (1/s).

X,Y are the two orthogonal flow modes (sine/cosine pair → oscillation) *Z* is the stress generated by the flow (e.g., viscoelastic response) σ controls the onset of instability (Hopf bifurcation) ; ω sets the oscillation frequency α indicates how stress damps the flow ; β shows how flow generates stress and δ indicates how fast stress relaxes.

5. Bifurcation Analysis and Optimal Control

5.1. Bifurcation Analysis

Bifurcation calculations are performed using the MATLAB software MATCONT. Bifurcation analysis explains the main causes for multiple steady-states and limit cycles. Branch points and limit points cause multiple steady-state solutions while limit cycles and oscillatory behavior are caused by Hopf bifurcation points. The MATLAB program that effectively locates limit points, branch points, and Hopf bifurcation points is MATCONT. This program was developed and improved by several researchers[26]. This program is very effective in identifying Limit points(LP), branch points(BP), and Hopf bifurcation points(H) for a system of ordinary differential equations

$$\frac{dx}{dt} = f(x, \alpha) \quad (27)$$

$x \in R^n$ where the bifurcation parameter is α . The gradient vector is orthogonal to the tangent and hence the tangent plane at any point $w = [w_1, w_2, w_3, w_4, ...w_{n+1}]$ must satisfy

$$Aw = 0 \quad (28)$$

The matrix **A** is defined by

$$A = [\partial f / \partial x \quad | \partial f / \partial \alpha] \quad (29)$$

The sub-matrix $\partial f / \partial x$ is the Jacobian matrix. For both limit and branch points, the Jacobian matrix $J = (\partial f / \partial x)$ must have a determinant of 0.

At a limit point, the $n+1^{th}$ component of the tangent vector $w_{n+1} = 0$. For a branch point,

the matrix $B = \begin{bmatrix} A \\ w^T \end{bmatrix}$ must be singular and have a determinant of 0.

At a Hopf bifurcation point,

$$\det(2f_x(x,\alpha)@I_n)=0 \tag{30}$$

@ indicates the bialternate product while I_n is the n-square identity matrix. Hopf bifurcations cause limit cycles and should be eliminated because limit cycles make optimization and control tasks very difficult. More details can be found in Kuznetsov and Govaerts respectively [27,28].

5.2. Optimal Control

Pyomo.dae is used for the Optimal Control calculations [29]. Pyomo.DAE is a powerful extension of the Pyomo optimization modeling framework, which is well-suited for solving dynamic systems of differential and algebraic equations. It is a symbolic environment for solving differential-algebraic equation systems in the context of optimization problems. This is very important in process systems engineering, chemical kinetics, and control systems, where the dynamic response of systems is of prime interest.

At its heart, Pyomo.DAE enables users to define time-varying variables, derivatives, and constraints symbolically, which can be easily integrated into a Pyomo model. Users can easily define continuous sets for time or other continuous variables, which can be used to define their derivatives over those sets. This symbolic approach enables users to easily discretize continuous differential-algebraic equation systems using finite difference, collocation, or orthogonal collocation methods, thereby transforming continuous differential equations into algebraic equations that can be solved with standard solvers. The framework can handle both initial-value problems and dynamic optimization problems. In dynamic optimization, Pyomo.DAE allows the formulation of time-dependent objective functions and constraints, which is particularly useful in optimal control, energy systems, and chemical process scheduling problems.

One of the major advantages of Pyomo.DAE is that it is compatible with the Pyomo ecosystem. This allows users to leverage existing solver interfaces, variable bounds, nonlinear constraints, and objective functions within a combined static and dynamic modeling framework. Furthermore, the symbolic framework makes it easier to perform model verification, automatic differentiation, and sensitivity analysis. Pyomo.DAE provides a flexible, extensible, and open-source environment for modeling, simulation, and optimization of dynamic systems. By integrating symbolic modeling of DAEs with powerful discretization and optimization capabilities, it provides a unique framework for solving complex time-dependent problems. Its tight integration with Pyomo enables the efficient solution of both simple and complex dynamic optimization problems, making it a cornerstone of modern computational modeling of dynamic systems. In Pyomo.DAE , the differential equations are converted to a Nonlinear Program (NLP) using the orthogonal collocation method. The NLP is solved using IPOPT [30].

6. Formation of Stability Dataset from MATCONT Results

A stability dataset was developed based on the results from numerical continuation calculations carried out in MATCONT. The stability dataset consists of rows, each representing a continuation point from an equilibrium branch. The columns in each row consist of the state variables, the bifurcation parameter, and a stability measure. The stability measure is a numerical value derived from the Jacobian matrix. The Jacobian matrix is computed numerically at each equilibrium point. The eigenvalues are then computed automatically using MATLAB. The maximum value of the real part of these eigenvalues is then computed as a scalar stability measure.

The stability measure is computed using “eig_real_max = max(real(eigvals));” in MATLAB. The stability measure is a quantitative metric in which negative values indicate locally asymptotically stable equilibria, positive values indicate instability, and a zero crossing indicates a Hopf bifurcation. The stability dataset is then saved as a CSV file. The dataset can then be used in subsequent computational calculations to perform classification or regression to identify stability boundaries or approximate bifurcations.

7. Neural Network Surrogate for Stability Prediction

Direct embedding of eigenvalue calculations into IPOPT-based optimal control is impractical for several reasons: (i) computing eigenvalues at each time step is computationally expensive, (ii) the mapping from states to the maximum eigenvalue is non-smooth near eigenvalue crossings, and (iii) symbolic differentiation of eigenvalues is challenging.

Prior to neural network training, all input variables were standardized to improve numerical conditioning and training stability. Let x_{raw} denote the vector of state variables and bifurcation parameter obtained from the stability dataset. For each input variable j, the training mean μ_j and training standard deviation σ_j were computed over the training dataset as the arithmetic mean and standard deviation, respectively. The training mean for the input variable j is defined as the arithmetic average over all training samples as $\mu_j=\frac{1}{N}\sum_{k=1}^{N}x_j^{(k)}$ and the training standard deviation for the input variable j is defined as: $\sigma_j=\frac{1}{N}(\sum_{k=1}^{N}x_j^{(k)}-\mu_j)^2$

The standardized inputs were defined as

$$x_j = \frac{x_{\text{raw},j} - \mu_j}{\sigma_j}.$$

This transformation ensures that each input variable has zero mean and unit variance over the training set, thereby improving neural network conditioning and gradient-based optimization performance. The vectors μ,σ μ and σ computed during training were stored and embedded identically within the Pyomo optimal control formulation to ensure consistency between neural network training and deployment. To overcome these limitations, a feedforward neural network is trained to approximate the maximum eigenvalue as a smooth function of the system state and bifurcation parameter. A typical architecture employs the hyperbolic tangent (tanh) as a smooth activation function. If the input vector is denoted by *x,* which are the scaled variables, then the network is defined as:

$$\begin{aligned} z1 &= tanh\left(W1\,x + b1\right) \\ z2 &= tanh\left(W2\,z1 + b2\right) \\ \lambda\_max\_NN &= W3\,z2 + b3 \end{aligned} \tag{31}$$

Because tanh is infinitely differentiable, the network is fully smooth, guaranteeing the availability of first and second derivatives required by IPOPT. Here, W1, W2, and W3 are the weights that scale and combine inputs or hidden-layer features, while b1, b2, and b3 are the biases that allow the neurons to shift their activation independently of the inputs. Without biases, the network output would be constrained to pass through the origin, limiting flexibility.

The hidden-layer outputs z1, z2, represent nonlinear combinations of the inputs and previous-layer features, respectively. Each element of z_1 is a smoothed combination of the original inputs, while each element of z2 encodes more abstract patterns extracted from *z*1. The final output λ_max_NN provides a smooth approximation of the maximum real eigenvalue, enabling efficient and differentiable stability evaluation within the optimal control problem. Fig. 1 shows a chart describing the computational strategy. The integration into optimal control is done using a soft penalty formulation where we use a smooth_max function that converts λ into a smooth, nonnegative penalty that only "activates" when the system is unstable:

$$s_{\max}(\lambda+\varepsilon_1) = smooth - \max(\lambda+\varepsilon_1) = \frac{(\lambda+\varepsilon_1)+\sqrt{(\lambda+\varepsilon_1)^2+\varepsilon_1}}{2} \tag{32}$$

λ is the neural network's predicted maximum eigenvalue at the current state and parameter, while ε is a small positive safety margin to ensure differentiability. The soft penalty formulation involves the new objective function, where the original objective function $optv(t) = (\sum (X(t))^2 + (Y(t))^2 + (Z(t))^2$ is modified to $\sum (optv(t) + \alpha_{hopf} . s_{\max}(\lambda+\varepsilon_1))^2$ α_{Hopf} controls how aggressively instability is penalized, and ε_1 prevents numerical issues at exactly λ = 0 and slightly shifts the stability boundary. This ensures differentiability for IPOPT and avoids non-smooth optimization.

8. Results

The Bifurcation analysis revealed a Hopf bifurcation at (X,Y,Z, σ) values of (0,0,0,0).
This is shown in Fig. 1a. The limit cycle that occurs because of this Hopf bifurcation is seen in Fig 1b. This corresponds to the onset of oscillatory convection, which in engineering systems may manifest as temperature oscillations or flow instabilities affecting heat transfer performance. For the optimal control, when no measures are taken ($\alpha_{hopf} = 0$), $(\sum optv(t))^2$ is minimized, and when the soft penalty formulation is integrated, $\sum (optv(t) + \alpha_{hopf} . s_{\max}(\lambda+\varepsilon_1))^2$ is minimized.

When no measures were taken the obtained value of $(\sum optv(t))$ was 0.02526 when the soft penalty formulation is integrated, with $\alpha_{hopf} = 5000;$ the obtained value of $(\sum optv(t))$ was 0.02854944762055029. This indicates that a small price has to be paid to add a soft penalty constraint. Figures 2a-2b show the optimal control profiles without Hopf bifurcation constraints and figures 2c-2d show the optimal control profiles with Hopf bifurcation constraints. The figures 2b and 2d show the control profiles. σsg is the smoothed out profile (using the Savitzky Golay filter) of the control profile σ.

9. Discussion of Results

The results obtained from the bifurcation analysis and optimal control formulation provide important insight into the dynamic behavior of soft-matter flows and the challenges associated with controlling systems near instability. The bifurcation analysis performed using MATCONT clearly identifies the presence of a Hopf bifurcation at the equilibrium point ((X,Y,Z,\sigma) = (0,0,0,0)). This result is significant because it confirms that the reduced-order model derived from the Navier–Stokes equations coupled with the constitutive law is capable of capturing oscillatory instabilities arising from the interaction between flow and stress dynamics. The emergence of a limit cycle beyond the Hopf point, as shown in Fig. 1b, demonstrates that the system transitions from a steady state to sustained oscillations. Physically, this corresponds to the onset of time-periodic behavior in soft matter systems, such as fluctuating stresses or oscillatory flow structures, which are commonly observed in viscoelastic fluids and colloidal suspensions.

The presence of a Hopf bifurcation has important implications for control. In engineering systems, such oscillations are often undesirable because they can degrade performance, reduce efficiency, or lead to instability in process operations. The optimal control problem was therefore formulated to regulate the system dynamics by manipulating the bifurcation parameter (\sigma(t)), which is physically related to flow conditions such as shear rate or Reynolds number. The baseline case, where no stability penalty is imposed, minimizes only the state energy. In this case, the resulting trajectories show that the system naturally evolves toward regions close to instability. The corresponding control profile exhibits relatively aggressive variations, reflecting the need to counteract the intrinsic tendency of the system to amplify perturbations near the bifurcation point.

When the soft stability penalty based on the neural network surrogate is introduced, a different behavior is observed. The neural network, trained on stability data generated from MATCONT, provides a smooth approximation of the maximum real part of the eigenvalues. This allows the stability constraint to be embedded within the optimal control problem solved using Pyomo.DAE without explicitly computing eigenvalues at each time step. The inclusion of this penalty modifies the objective function such that unstable regions are discouraged during optimization. As a result, the controlled trajectories remain closer to the stable region of the phase space, avoiding excursions into oscillatory regimes.

The quantitative comparison between the two cases highlights the trade-off between performance and stability. The objective value increases slightly from 0.02526 to approximately 0.02855 when the stability penalty is included. This increase represents the “cost of stability,” indicating that maintaining the system in a stable regime requires additional control effort or deviation from the optimal unconstrained trajectory. However, this increase is relatively small, suggesting that stability can be enforced without significantly compromising performance. This is an important practical result, as it demonstrates that stability-aware control strategies can be implemented with minimal penalty in objective value.

Another key observation is the change in the control profile (\sigma(t)). In the absence of the stability constraint, the control signal exhibits sharper variations, reflecting the optimizer’s attempt to minimize the objective without regard to stability. In contrast, when the stability penalty is included, the control profile becomes smoother, particularly after applying the Savitzky–Golay filter. This smoothing effect is important because it indicates that the system is being guided away from regions where rapid changes in control would otherwise be required to counteract instability. From a practical standpoint, smoother control inputs are desirable because they are easier to implement in real systems and reduce actuator wear.

The use of a neural network surrogate for stability prediction is a particularly noteworthy aspect of this work. Direct computation of eigenvalues within an optimal control framework is computationally expensive and can introduce non-smoothness, which is problematic for gradient-based solvers such as IPOPT. By replacing the eigenvalue calculation with a differentiable surrogate model, the optimization problem remains smooth and tractable. At the same time, the surrogate retains sufficient accuracy to capture the stability boundary, as evidenced by the consistent behavior of the controlled system relative to the bifurcation point.

Overall, the results demonstrate that the combination of reduced-order modeling, bifurcation analysis, and machine-learning-assisted optimal control provides a powerful framework for analyzing and controlling soft-matter systems. The ability to detect and avoid Hopf bifurcations in a computationally efficient manner is particularly valuable for applications involving viscoelastic flows, where instability can have significant operational consequences. The methodology developed here can be extended to more complex systems, including higher-dimensional models and spatially distributed flows, making it a promising approach for future research in soft matter and fluid dynamics.

10. Conclusions and Future Work

This work presents a unified framework for analyzing and controlling oscillatory instabilities in soft matter systems by combining reduced-order modeling, bifurcation analysis, and optimal control. Starting from the governing equations of viscoelastic flow, a low-dimensional dynamical system was derived using Galerkin projection and further reduced using center manifold concepts to capture the essential

features near a Hopf bifurcation. The analysis confirmed the existence of a critical parameter regime in which the system transitions from a stable equilibrium to sustained oscillations, highlighting the fundamental role of flow–stress coupling in generating complex dynamics.

An optimal control formulation was then developed in which the bifurcation parameter was treated as a time-dependent control input. By incorporating a stability-aware objective, including a smooth surrogate for the system's stability boundary, the framework successfully guided the system away from unstable regimes while maintaining acceptable performance. The results demonstrate that it is possible to regulate soft matter flows in a way that balances stability and control effort, providing a practical pathway for managing nonlinear dynamics in engineering applications.

Future work will focus on several key extensions. First, the incorporation of rigorous eigenvalue-based constraints within the optimal control problem will provide a more direct connection to bifurcation theory. Second, the methodology can be extended to higher-dimensional and spatially distributed systems, allowing for more realistic representations of soft matter flows. Third, improved data-driven models, including physics-informed neural networks, may enhance the accuracy and interpretability of stability predictions. Finally, experimental validation and real-time control implementation remain important directions for translating these theoretical developments into practical applications in chemical engineering and soft matter processing systems.

Data Availability Statement

All data used is presented in the paper

Conflict of interest

The author, Dr. Lakshmi N Sridhar has no conflict of interest.

Acknowledgement

Dr. Sridhar thanks Dr. Carlos Ramirez for encouraging him to write single-author papers.

References

1. Datta, S.S., Grier, D.G. (2020). Confinement and nonlinear dynamics in soft colloidal systems. *Soft Matter,* 16, 6105–6116.
2. Saint-Michel, B., Manneville, P. (2020). Instabilities in viscoelastic channel flows. *Journal of Fluid Mechanics*, 889, A30.
3. Lopez-Barron, C.R., Wagner, N.J. (2020). Structure–property relations in complex fluids. *Journal of Rheology*, 64, 625–643.
4. Haward, S.J., McKinley, G.H. (2021). Instabilities in viscoelastic flows. *Annual Review of Fluid Mechanics*, 53, 259–284.
5. Fielding, S.M. (2021). Shear banding in soft glassy materials. *Reports on Progress in Physics*, 84, 102601.
6. Steinberg, V. (2021). Elastic turbulence in polymer solutions. *Nature Reviews Physics, 3,* 401–412.
7. Zhang, Y., Arratia, P.E. (2021). Flow instabilities in complex fluids. *Physical Review Fluids, 6*, 110501.
8. Divoux, T., Fardin, M.A., Manneville, S. (2021). Rheological chaos in soft matter. *Annual Review of Fluid Mechanics, 53*, 181–210.
9. Ovarlez, G., Cohen-Addad, S. (2021). Yield stress fluids and flow instabilities. *Journal of Rheology, 65*, 1141–1164.
10. Qin, B., Arratia, P.E. (2022). Elastic instabilities in viscoelastic flows. *Physical Review Fluids, 7*, 033301.
11. Fraggedakis, D., et al. (2022). Nonlinear dynamics in viscoelastic flows. *Journal of Fluid Mechanics,* 939, A17.
12. Datta, S.S. (2022). Microscopic origins of soft matter flow behavior. *Soft Matter*, 18, 577–592.
13. Walkama, D.M., et al. (2022). Instabilities in confined soft matter flows. *Physical Review Fluids,* 7, 093302.
14. Li, Y., Zhang, H. (2022). Bifurcation in complex fluids. *Chaos*, 32, 093115.
15. Perge, C., et al. (2022). Dynamics of colloidal suspensions under flow. *Soft Matter,* 18, 8375–8387.
16. Saint-Michel, B., et al. (2023). Elastic instabilities in Couette flow. *Journal of Fluid Mechanics,* 955, A12.
17. Boudara, V.A.H., et al. (2023). Nonlinear viscoelastic flow instabilities. *Physical Review Fluids*, 8, 013302.
18. Datta, S.S., et al. (2023). Flow-induced structures in soft materials. *Nature Physics,* 19, 1112–1120.
19. Song, Y., et al. (2023). Machine learning for soft matter rheology. *Soft Matter*, 19, 4567–4580.
20. Liu, Y., et al. (2023). Neural network modeling of viscoelastic flows. *Journal of Non-Newtonian Fluid Mechanics*, 315, 104995.
21. Gupta, R., et al. (2024). Data-driven modeling of soft matter dynamics. *Soft Matter*, 20, 1123–1138.
22. Morozov, A., van Saarloos, W. (2024). Subcritical instabilities in viscoelastic flows. *Physics Reports,* 1000, 1–75.
23. Arratia, P.E., et al. (2024). Advances in elastic turbulence. *Annual Review of Fluid Mechanics,* 56, 245–270.
24. Zhang, X., et al. (2024). Stability of viscoelastic channel flows. *Journal of Fluid Mechanics*, 978, A45.
25. Singh, A., et al. (2025). Optimal control of instabilities in soft matter flows. *Chemical Engineering Science*, 285, 119876.
26. Dhooge, A., Govearts, W., and Kuznetsov, A. Y. (2003). MATCONT: A Matlab package for numerical bifurcation analysis of ODEs, *ACM transactions on Mathematical software* 29(2) pp. 141-164.
27. Kuznetsov, Y. A. (1998). Elements of applied bifurcation theory. *Springer*, NY.
28. Govaerts, w. J. F. (2000). Numerical Methods for Bifurcations of Dynamical Equilibria", *SIAM*.

29. Hart, W. E., Laird, C. D., Watson, J. P., Woodruff, D. L., Hackebeil,G .A., Nicholson, B. L., Siirola, J. D. “Pyomo – Optimization Modeling in Python” Second Edition. Vol. 67.
30. Wächter, A., Biegler, L. (2006). On the implementation of an interior-point filter line-search algorithm for large-scale nonlinear programming”. *Math. Program*. 106, 25–57.

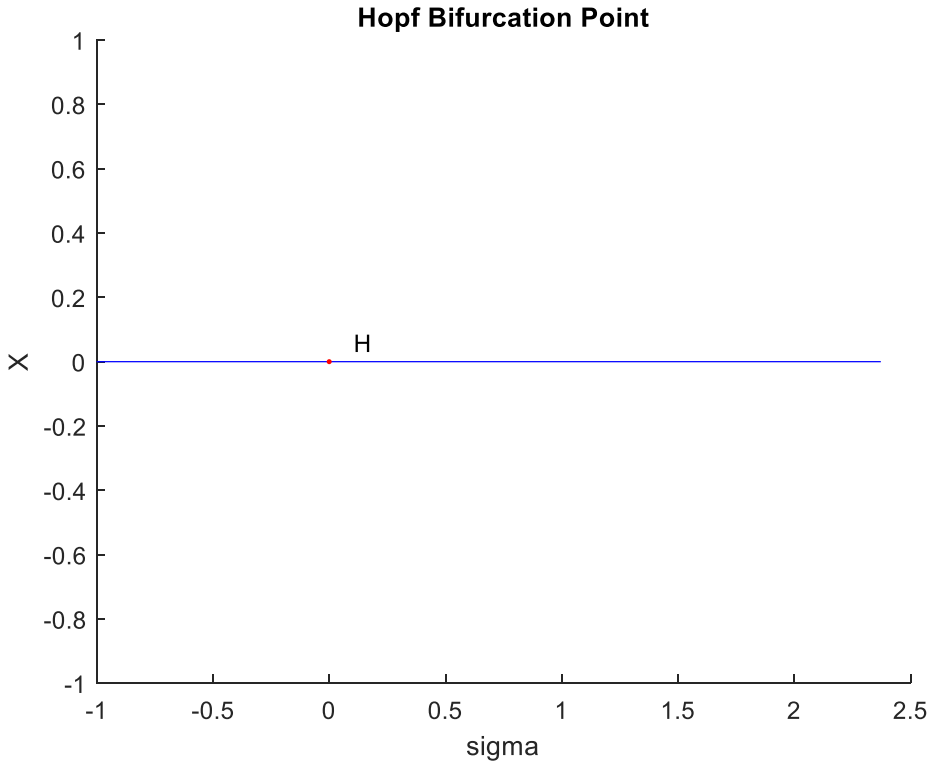

Figure 1(a): Hopf Bifurcation Point

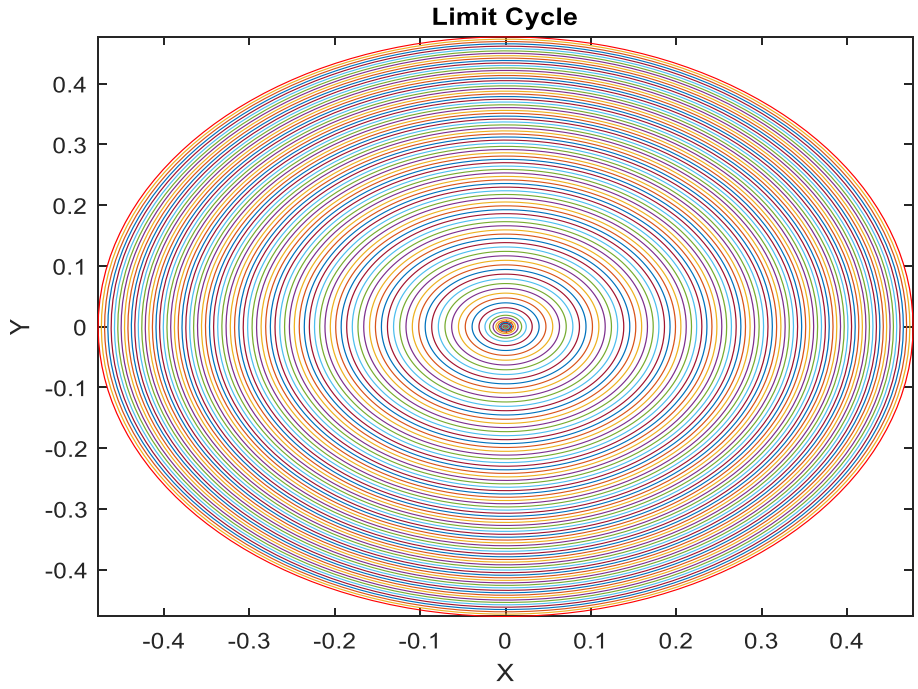

Figure 1(b): Limit Cycle caused by Hopf Bifurcation Point

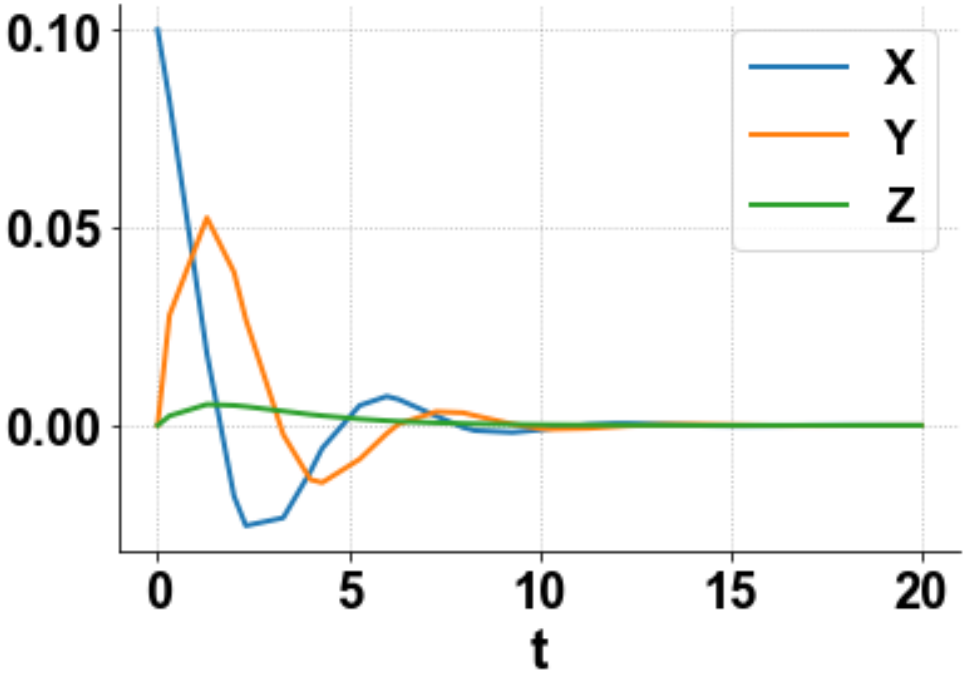

Figure 2(a): Optimal Control X, Y, Z Profiles with no Hopf Constraint

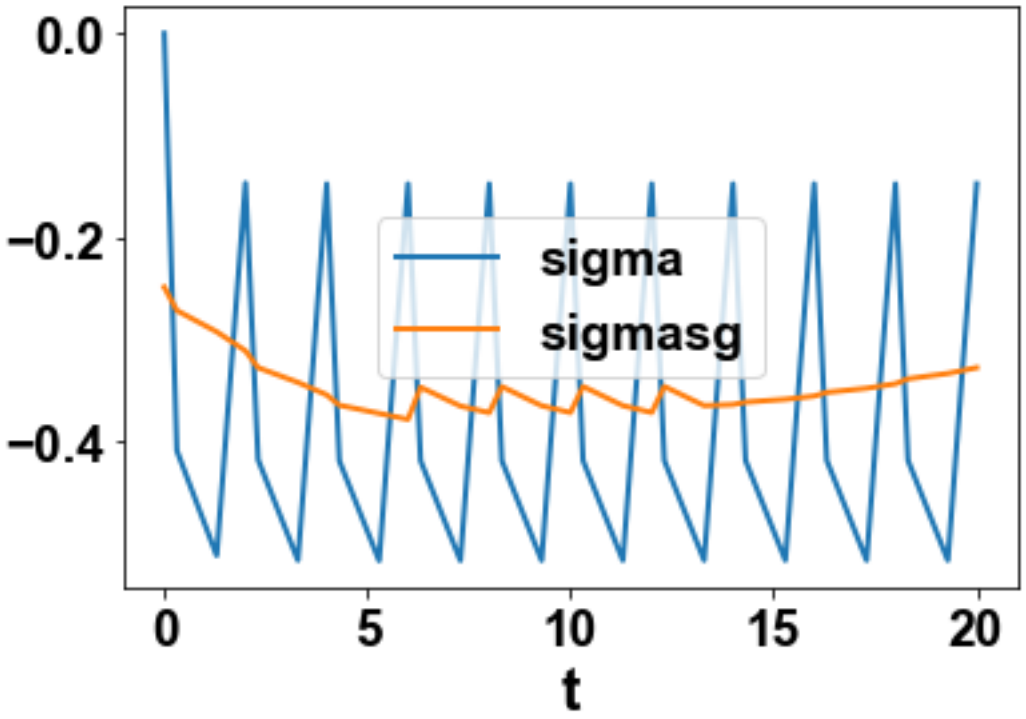

Figure 2(b): Optimal Control $\sigma, \sigma sg$ Profiles with no Hopf Constraint

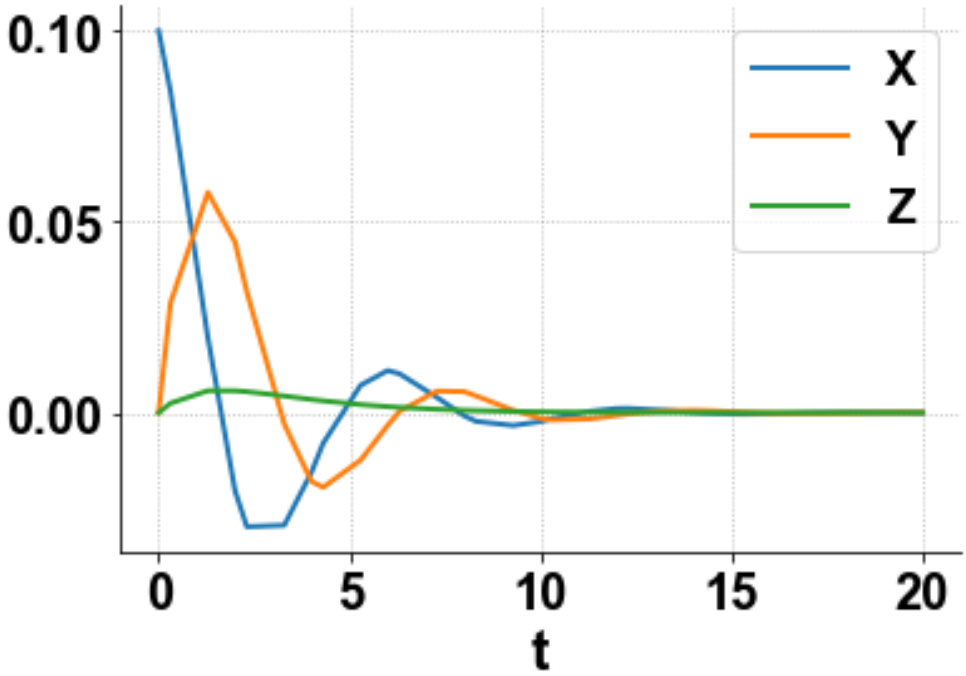

Figure 2(c): Optimal Control X, Y, Z Profiles with Hopf Constraint

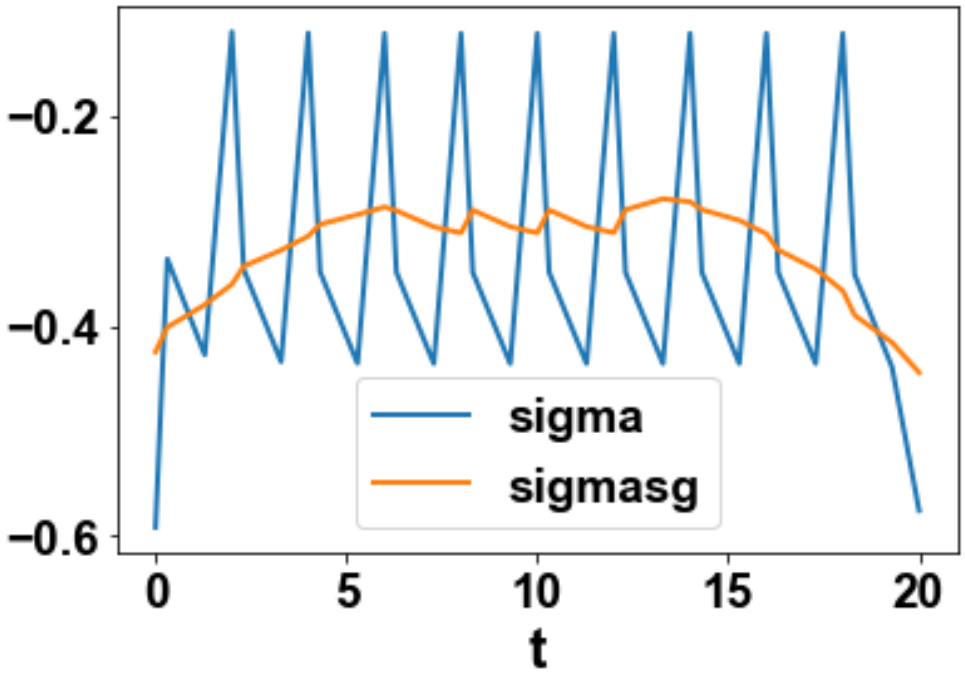

Figure 2(d): Optimal Control $\sigma, \sigma sg$ Profiles with no Hopf Constraint